ELSEVIER

Earth and Planetary Science Letters 188 (2001) 349–367

EPSL

www.elsevier.com/locate/epsl

Geochemical heterogeneity within mid-ocean ridge lava flows: insights into eruption, emplacement and global variations in magma generation

K.H. Rubin [a,*], M.C. Smith [a], E.C. Bergmanis [a], M.R. Perfit [b], J.M. Sinton [a], R. Batiza [a,c]

[a] Department of Geology and Geophysics, University of Hawaii, Honolulu, HI 96822, USA
[b] Department of Geological Sciences, P.O. Box 112120, Williamson Hall, University of Florida, Gainesville, FL 32611, USA
[c] MGG Division of Ocean Sciences, National Science Foundation, 4201 Wilson Blvd., Arlington, VA 22230, USA

Received 5 September 2000; accepted 28 March 2001

Abstract

Compositional heterogeneity in mid-ocean ridge (MOR) lava flows is a powerful yet presently under-utilized volcanological and petrological tracer. Here, it is demonstrated that variations in pre- and syn-eruptive magmatic conditions throughout the global ridge system can be constrained with intra-flow compositional heterogeneity among 10 discrete MOR flows. Geographical distribution of chemical heterogeneity within flows is also used along with mapped physical features to help decipher the range of conditions that apply to seafloor eruptions (i.e. inferred vent locations and whether there were single or multiple eruptive episodes). Although low-pressure equilibrium fractional crystallization can account for much of the observed intra-flow compositional heterogeneity, some cases require multiple parent magmas and/or more complex crystallization conditions. Globally, the extent of within-flow compositional heterogeneity is well correlated (positively) with estimated erupted volume for flows from the northern East Pacific Rise (EPR), and the Mid Atlantic, Juan de Fuca and Gorda Ridges; however, some lavas from the superfast spreading southern EPR fall below this trend. Compositional heterogeneity is also inversely correlated with spreading rate. The more homogeneous compositions of lavas from faster spreading ridges likely reflect the relative thermal stability and longevity of sub-ridge crustal magma bodies, and possibly higher eruption frequencies. By contrast, greater compositional heterogeneity in lavas at slower spreading rates probably results from low thermal stability of the crust (due to diminished magma supply and greater hydrothermal cooling). Finally, the within-flow compositional variations observed here imply that caution must be exercised when interpreting MOR basalt data on samples where individual flows have not been mapped because chemical variations between lava samples may not necessarily record the history of spatially and temporally distinct eruptions.

Keywords: eruptions; lava flows; igneous rocks; geochemistry; magmas; mid-ocean ridge basalts; petrology; submarine volcanoes; volcanism

* Corresponding author. Tel.: +1-808-956-8973; Fax: +1-808-956-5512; E-mail: krubin@soest.hawaii.edu

0012-821X/01/$ – see front matter
PII: S0012-821X(01)00339-9

1. Introduction and background

Mid-ocean ridges (MORs) are dynamic volcanic environments. Although remote and difficult to observe, MOR volcanism produces lavas that cover roughly 2/3 of Earth's surface, and MOR crust is an important chemo-physical interface between the mantle, ocean, and marine biosphere (e.g. [2–4]).

To completely understand the physical and chemical history of MORs, it is important to study them over a range of temporal and geographic length scales, including those related to the emplacement of individual eruptive units. MOR lava flows, like those in other volcanic terrains, have complex emplacement histories and preserve information about processes from initial melt generation to post-emplacement cooling. Through comparisons of individual flows from different MORs, intra-flow compositional heterogeneity is used here to constrain variations in magmatic/petrologic conditions through the global ridge system. Furthermore, the spatial distribution of chemical heterogeneity within a flow is used along with mapped physical features to help decipher the cryptic history and range of conditions that apply to eruption and emplacement of specific submarine lava flows.

Numerous studies of MOR basalt (MORB) compositions over the past four decades have provided insights into the formation of the oceanic lithosphere and, because MORB is largely unaffected by crustal contamination, how mantle compositions/heterogeneities are sampled by volcanism (e.g. [5–7] and references therein). However, MOR data have mostly been collected at coarse/incompletely resolved length and spreading time scales (10 s of km and kyr), without the benefit of detailed geological maps needed to place volcanic and other structures in the context of individual eruptions. MOR volcanoes are relatively inaccessible and are primarily sampled from surface ships (e.g. wax coring or rock dredging), which is broadly equivalent to sampling Hawaiian volcanoes from a helicopter flying at 2 km altitude. Only a small percentage of MORB samples in the literature have been collected using in situ observation (by submersible or ROV), and only a fraction of those have the geologic information necessary to place them within the context of a specific eruption.

Since the earliest studies of oceanic volcanism, MORBs have been known to be less compositionally variable than lavas from other Earthly volcanic terrains (including subaerial sites of primarily tholeiitic extrusion). The lack of broad compositional variability coupled with the difficulty in obtaining samples with a clearly defined context has resulted in spatial variation in compositions of individual MORB samples commonly being used literally to ascribe spatial and/or temporal variability to petrogenetic processes and/or mantle compositions. There has been little attempt to distinguish petrogenetic heterogeneity between flows from heterogeneity within a flow. Yet, the significance of broader scale spatial and temporal variations in lava composition cannot be completely assessed without understanding both the effects of the eruptive process itself (in terms of creating or destroying magmatic compositional variability) and the extent to which the compositional variability in MORB is accounted for by pre- and post-eruptive petrologic histories of single eruptive units.

An active MOR eruption has yet to be witnessed. Still, the range of geomorphic features that constitute an individual submarine lava flow have recently begun to be recognized through a combination of detailed near-bottom surveying, active monitoring and fortuitous arrival at the scene of recent volcanism (e.g. [8–12]). Such features are easiest to identify in very recent lavas because weathering and sedimentation can rapidly obscure flow contacts between older lavas. As a result, the database of mapped discrete submarine lava flows (or flow sequences) is still small and limited primarily to young flows (e.g. [7,13]). We know little of the composition, mode of emplacement or aerial extent of $>99\%$ of the lava flows within even the most active/youngest region of the global MOR system. In most cases, there are inadequate vertical cross-sectional exposures with which to identify physical variations arising from multiple emplacement lobes [14] and inflation/cooling episodes [15]. Instead, MOR flows are typically observed and sampled from the

upper crust or in collapse features. Nevertheless, detailed study of the MOR lava flow database provides useful, albeit preliminary, insights into MOR processes.

2. Compositional heterogeneity of subaerial and MORB lava flows

Physically, most lava flows are complex, with few, if any, known examples of a simple basaltic flow (one that is not divisible into flow units having distinguishable extrusion and cooling histories [14]). Not surprisingly, their compound character leads to small-scale internal compositional variations. Early works on subaerial basalt flows defined heterogeneity by variations in phenocryst populations (e.g. [14,16]) and liquid chemistry (e.g. [16–18]), and led some authors to caution against characterizing lava flow composition with only one or a few samples. Such heterogeneity was attributed to a combination of emplacement mechanism, assimilation, flow differentiation, in situ fractionation, localized oxidation, zoned magma chambers and random mixing. These early studies also noted that although only loosely quantified, analytical errors contribute to apparent heterogeneity between multiple samples of a flow.

The first systematic attempt to quantify 'extra-analytical' chemical heterogeneity in lava flows and to evaluate the source(s) of this compositional variability examined 16 historical basaltic eruptions from 1843 to 1975 at Mauna Loa, Hawaii, USA, using a measure known as the 'homogeneity index' (HI) [1]. The HI uses multiple chemical constituents in different lava flow samples, normalized by the precision to which they can be measured. It is defined as:

$$\mathrm{HI} = \frac{\Sigma(S_i)/(P_i)}{n}$$

where S_i and P_i are the standard deviation (2σ) about the mean and analytical precision for element i, and n is the number of elements used. Precision is quantified by replicate analyses on a single sample or standard that is similar in composition to the unknowns. An index value of ≤ 1 implies no compositional heterogeneity outside of analytical uncertainty. Higher values indicate analytically significant compositional variation. HI is referred to here as the 'heterogeneity index', since this name seems more appropriate for an index for which larger values correspond to greater compositional variance.

The original HI study included 10 major elements (Si, Ti, Al, Fe, Mn, Mg, Ca, Na, K, P) and seven trace elements (Nb, Zr, Sr, Zn, V, Ni, Cr) analyzed by XRF on 80–100 g rock powders of 5–12 samples per Mauna Loa flow [1]. HI ranged from 1.1 to 13.9, except for picrite eruptions in 1852 (HI = 30.3) and 1868 (HI = 34.0) that had copiously accumulated olivine. Compositional variability was not a simple function of emplacement rate or time, but larger area flows were typically more heterogeneous [1]. Roughly 50% and $\sim$85% of the compositional heterogeneity in the non-picrites and the picrites could be mathematically 'eliminated' by correcting to constant MgO for low-pressure crystal fractionation or accumulation (with only olivine on the liquidus) [1]. The remaining heterogeneity (HI = 1–5) was presumed to reflect other processes. Some Kilauea lavas with smaller flow areas were also noted to be more heterogeneous than those at Mauna Loa, suggesting that these other processes were related to the scale and complexity of crustal magma reservoirs at both volcanoes [1].

As on land, compositional variability in a MORB flow can reflect spatial/temporal variability in source composition, melting, crystallization/assimilation histories, and evolution during emplacement. Previous studies of individual MOR lava flows [7,10,13,19–27] suggest that compositional ranges within a single flow can be substantial relative to the range of compositions along its respective ridge segment (i.e. Fig. 1), and element–element variations within MOR flows do not always follow expected crystallization trends (e.g. smooth variations with MgO).

Intra-flow compositional variability in MORB was discussed qualitatively using the variance of individual chemical elements in Icelandic [28] and submarine [7,24] lava flows. Later, HI was used to make the first quantitative comparison of the

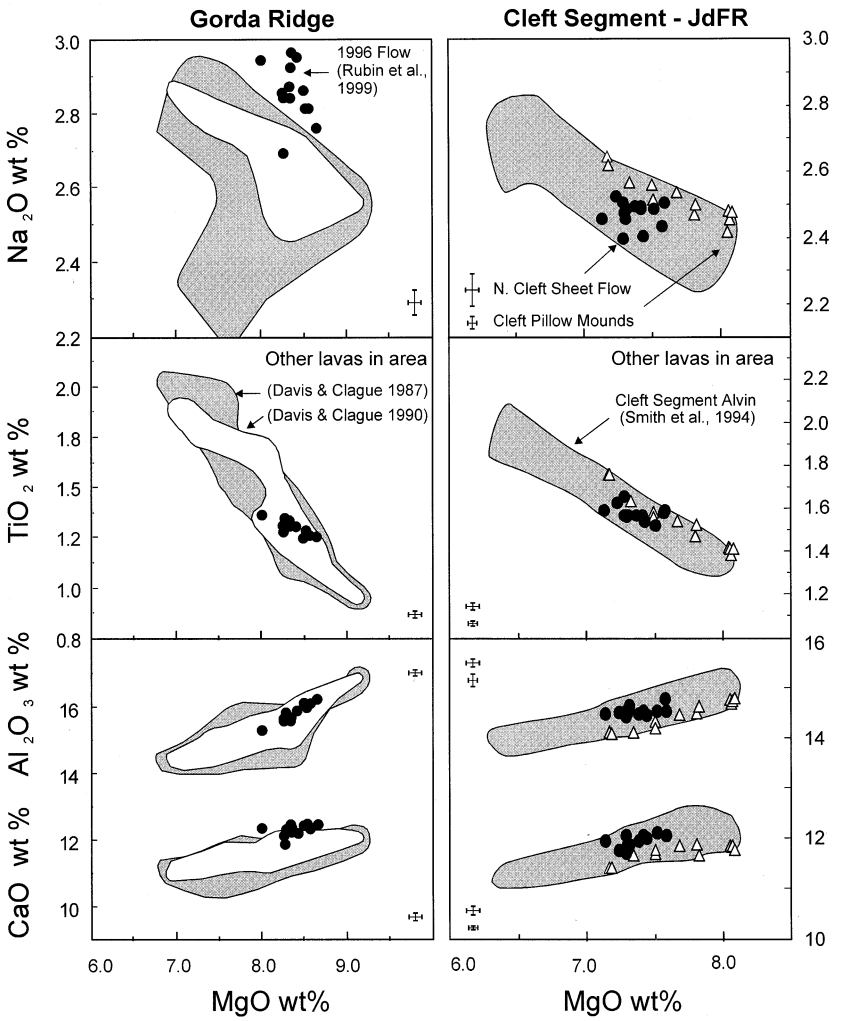

Fig. 1. Major element oxide compositions plotted versus MgO content for three individual MOR lava flows from the NE Pacific Ocean. Individual flow data are shown as filled circles (1996 N. Gorda Ridge and uncertain-aged N. Cleft Sheet flow) and open triangles (mid 1980s Cleft Pillow Mounds). Typical 2σ errors are depicted by the cross symbol in each panel. Filled fields represent 'whole ridge segment' compositional data from the vicinity of these lava flows for comparison (references given in the figure). Details about these and other MOR flows discussed in this paper are given in the **EPSL Online Background Dataset**[1].

compositional variability within a newly erupted (1996) lava flow on the North Gorda Ridge and five other discrete MORB lava flows from the literature [26]. HI values were based on 8–24 samples per flow, using electron microprobe major element glass analyses (trace element data were not used because they were not available for all flows). The pre-eruptive histories of those MOR magmas were found to be generally more variable as erupted volume increased, as indicated by a strong linear correlation of HI and flow volume ($R^2 > 0.95$), despite potential errors in estimating both parameters (discussed below). The spatial scales and compositional attributes of the intra-flow heterogeneity were not discussed. The fields for MORB and Mauna Loa overlap on a HI versus estimated flow volume plot [26], although the Mauna Loa field extends to greater values of each (Mauna Loa flow volumes from [29] and HI from [1,30]).

Table 1
Physical and compositional data for some MOR lava flows

Flow name	Location	Reference	Volume (10^6 m^3)	Number of samples		SiO_2	TiO_2	Al_2O_3	FeO	MnO	MgO	CaO	Na_2O	K_2O	P_2O_5	HI
1996 N. Gorda	Gorda 42°40′N	a, 1	18	12	mean wt%	51.04	1.26	15.81	8.57	0.13	8.37	12.26	2.85	0.10	0.11	2.06
					S_i (2σ)	0.56	0.09	0.54	0.41	0.02	0.35	0.34	0.15	0.01	0.02	
					P_i (2σ)	0.27	0.03	0.18	0.18	0.02	0.15	0.23	0.07	0.01	0.01	
1991-2 BBQ	EPR 9°50′N	b, 2	5	21	mean wt%	49.97	1.27	15.51	9.32	0.18	8.54	12.20	2.57	0.10	0.14	1.55
					S_i (2σ)	0.30	0.06	0.25	0.23	0.02	0.32	0.11	0.13	0.03	0.06	
					P_i (2σ)	0.38	0.06	0.13	0.18	0.02	0.14	0.13	0.12	0.01	0.02	
ODP	EPR 9°30′N	c, 3	0.03	8	mean wt%	50.39	1.66	14.39	10.58	0.20	7.08	11.90	2.60	0.14	0.13	1.26
					S_i (2σ)	0.21	0.03	0.14	0.10	0.02	0.08	0.03	0.06	0.005	0.01	
					P_i (2σ)	0.31	0.05	0.14	0.20	0.02	0.13	0.16	0.09	0.02	0.02	
N. Cleft 'Young Sheet Flow'	JdFR 44°56′N	d, 4	10.5	12	mean wt%	50.28	1.57	14.49	10.80	n.a.	7.38	11.95	2.47	0.14	0.15	2.04
					S_i (2σ)	0.75	0.07	0.18	0.37	n.a.	0.26	0.30	0.08	0.03	0.02	
					P_i (2σ)	0.25	0.02	0.25	0.22	n.a.	0.13	0.07	0.04	0.02	0.04	
1993 Coaxial	JdFR 46°31′N	e, 5	8.7	24	mean wt%	50.48	1.68	13.55	12.77	0.24	6.73	11.32	2.67	0.12	0.15	1.64
					S_i (2σ)	0.23	0.05	0.19	0.21	0.02	0.11	0.11	0.06	0.01	0.02	
					P_i (2σ)	0.25	0.02	0.10	0.09	0.01	0.08	0.17	0.08	0.01	0.01	
Serocki Volcano	MAR 22°55′N	f, 6	60	22	mean wt%	50.04	1.68	15.84	9.98	n.a.	7.50	11.20	2.94	0.14	0.17	3.27
					S_i (2σ)	0.61	0.24	0.70	0.82	n.a.	0.62	0.29	0.14	0.03	0.05	
					P_i (2σ)	0.37	0.07	0.08	0.22	n.a.	0.11	0.16	0.09	0.03	0.03	
Animal Farm	EPR 18°37′S	g, 7	200	53	mean wt%	50.57	1.66	14.45	10.57	0.20	7.27	11.72	2.96	0.09	0.14	1.20
					S_i (2σ)	0.29	0.05	0.19	0.20	0.02	0.13	0.14	0.08	0.01	0.01	
					P_i (2σ)	0.29	0.06	0.18	0.16	0.02	0.15	0.14	0.11	0.00	0.01	
Aldo-Kihi	EPR 17°30′S	h, 8	140	51	mean wt%	50.25	1.53	14.77	9.93	0.18	7.88	12.20	2.53	0.11	0.13	2.00
					S_i (2σ)	0.45	0.13	0.42	0.42	0.02	0.40	0.27	0.17	0.02	0.02	
					P_i (2σ)	0.28	0.05	0.12	0.24	0.03	0.14	0.14	0.12	0.01	0.01	
Moai	EPR 18°11′S	i, 9	26	11	mean wt%	49.78	1.35	15.36	9.62	0.18	8.12	12.52	2.62	0.08	0.11	1.62
					S_i (2σ)	0.27	0.10	0.25	0.32	0.02	0.27	0.18	0.17	0.01	0.02	
					P_i (2σ)	0.29	0.05	0.12	0.16	0.02	0.10	0.19	0.14	0.01	0.01	
N. Cleft Pillow Mounds	JdFR 45°05′N	j, 10	55	12	mean wt%	50.64	1.54	14.45	10.54	0.20	7.69	11.73	2.52	0.18	0.14	3.05
					S_i (2σ)	0.24	0.26	0.55	0.90	0.02	0.69	0.33	0.14	0.02	0.04	
					P_i (2σ)	0.43	0.03	0.15	0.13	0.01	0.19	0.17	0.11	0.02	0.02	

All data collected by electron microprobe analysis of glass chips (five spots per sample except 1996 N. Gorda samples, which are three spots per sample). Location/volume references (letters): a. [27]; b. [26]; c. (see **EPSL Online Background Dataset**[1]); d. [22]; e. [27]; f. [23]; g–i. [13]; j. [27]. Composition references (numbers): 1. [28]; 2. [7] and Perfit, unpublished; 3. (see **EPSL Online Background Dataset**[1]); 4. [29]: 5. [29]; 6. [21]; 7–9. [13] and Bergmanis et al., unpublished data; 10. [42] and Smith et al., unpublished data. Additional metadata can be found in the **EPSL Online Background Dataset**[1].

2.1. The MORB HI dataset

A small, 10 lava flow dataset forms the basis of the present study. Four mapped lava flows have been added since our initial investigation [26]: the mid 1980s Cleft Pillow Mounds eruption on the Juan de Fuca Ridge (JdFR) [8] and three representatives from a group of recently mapped flows on the superfast spreading southern East Pacific Rise (S-EPR) [13]. HI, location and volume data for each flow are in Table 1; physical, compositional and age metadata are in table 1 in the **EPSL Online Background Dataset**[1]. Flow volumes are very difficult to accurately estimate [7]. Volumes (from the literature) were derived from either (flow area)×(estimated thickness), depth-difference anomalies before and after eruption, or both. Generally, flow area can be constrained to within 10–20% error by mapped boundaries (W. Chadwick, personal communication). There can be more error in volume from thickness estimates (potentially 50–100%) and unaccounted for internal porosities (which locally can be up to 70%, largely hidden beneath the upper crusts of some flows from lava drain-out during emplacement). Propagated, these individual (maximum) errors result in potential volume uncertainties of ~85–125%.

Adding the Cleft Pillow Mounds to the previous HI database improves the correlation with estimated flow volume ($R^2 = 0.964$; Fig. 2a). Two of three S-EPR flows have significantly lower compositional heterogeneity for their volume; however, they do lie within the broad range of historical Mauna Loa lavas (Fig. 2b). The largest S-EPR flow ('Animal Farm') is very compositionally homogeneous (HI = 1.20) and would fall off the Fig. 2a trend even if the volume were erroneously large by 300% (which is outside of the uncertainty discussed above). This result is interpreted in a later section.

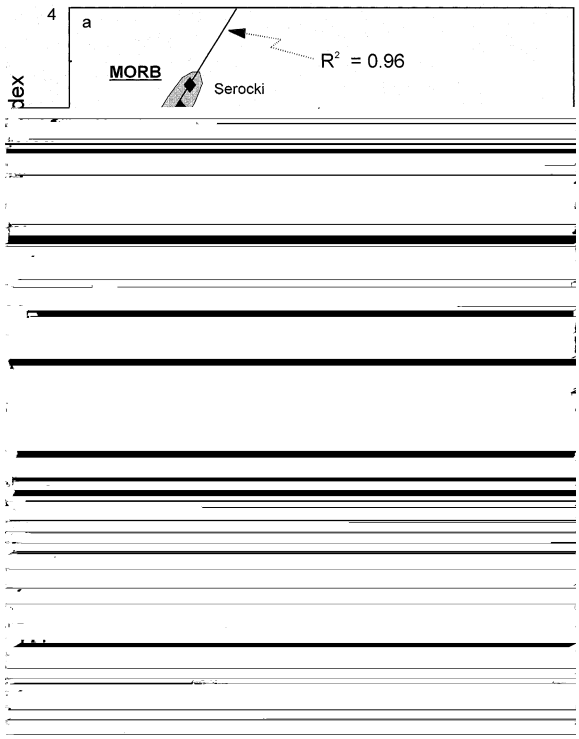

Fig. 2. (a) HI (defined in the text) versus estimated flow volume for 10 individual MOR lava flows. Note the high degree of correlation for all seven flows (filled diamonds) from locales other than the superfast spreading S-EPR (open squares). Two of three flows from the latter area are significantly less compositionally heterogeneous. (b) The range of MORB values relative to subaerial tholeiitic rift zone lavas. For comparison, 14 historical lavas from Mauna Loa volcano plus the ongoing Puu Oo eruption of Kilauea volcano (both in Hawaii) are plotted as data points, and our estimate of the range of tephras from the 1783–1784 Laki eruption (in Iceland) is plotted as a vertical bar (data sources described in the text). Note that despite the considerable scatter, the broad relationship between estimated flow volume and compositional heterogeneity is similar for the Hawaiian, Icelandic and MOR datasets.

3. Quantifying compositional heterogeneity

Before interpreting the MORB HI results, it is important to address the appropriateness and accuracy of the index for measuring true compositional variability within a flow. The logic of using multiple chemical elements is that the HI then integrates over a range of processes that might affect individual elemental abundances in varying

[1] http://www.elsevier.nl/locate/epsl; mirror site: http://www.elsevier.com/locate/epsl

proportion. Mapping lava flow compositional heterogeneity onto a single variable is useful for examining temporal–spatial evolution of an eruption, but study of individual element variations is also necessary to determine the source(s) of the heterogeneity.

True analytical precision is difficult to constrain, yet consideration of such uncertainty in a dataset is preferable to using 'raw' data to examine 'true' compositional signals. A rigorous method of accounting for analytical uncertainty is particularly important where compositional variance between and within flows is small relative to analytical error (i.e. most MORB) and when comparing data produced by different laboratories exhibiting a range of instrumental and analytical qualities (i.e. the case here). Reproducibility analyses of standard materials that are similar in composition to the unknowns are probably the best uncertainty measure. Instrument-related variability can affect precision even when a single operator makes analyses on a sample suite over only a few months, so 'P_i' values are best constrained simultaneous to unknowns analysis using at least as many standard measurements as unknown measurements. 'Historical' laboratory precision values (accumulated over a longer time period) are not as desirable because instrument drift that does not apply to a particular set of unknowns might occur (note slight variations in standards reproducibility between groups of analyses made over 4 months at the University of Hawaii in the Animal Farm, Aldo-Kihi and Moai data, Table 1).

It is important to investigate if analytical error correction using P_i is introducing uncertainty or biases into the data. In this MORB dataset, precision-normalization had minimal effect on the relative apparent compositional heterogeneity of individual elements (2σ): non-precision-normalized (i.e. S_i) and precision-normalized (i.e. S_i/P_i) data are well to moderately well correlated for most elements in Table 1 (S_i vs. S_i/P_i of Mg, Ti, Fe, Al, Si have $R^2 = 0.7$–0.85 and Ca, P have $R^2 = 0.5$). However, a few elements are only poorly correlated (Na, K, Mn have $R^2 < 0.2$). An index of combined non-precision-normalized elemental heterogeneity (e.g. $\Sigma S_i/n$, which we term 'np-HI') is not well correlated with HI ($R^2 = 0.38$; Fig. 3a), although this is dominated by non-systematic variations in three typically low-precision elements (Mn, P and K). Removing

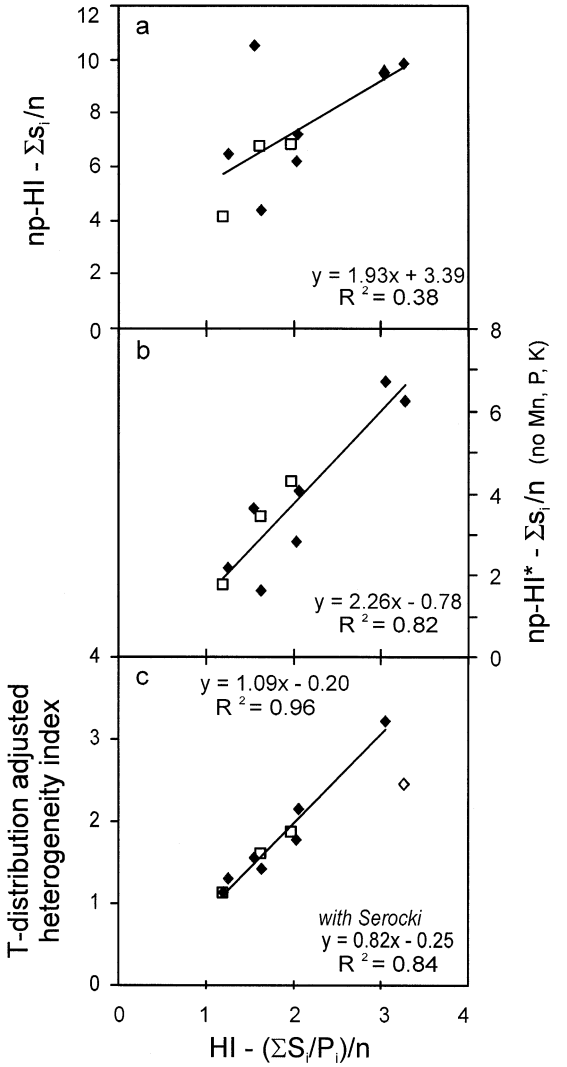

Fig. 3. Various other means of estimating chemical heterogeneity plotted versus the HI (symbols as in Fig. 2). a: Np-HI (index of non-precision-normalized standard deviations, S_i, for all 10 basaltic major elements). b: Np-HI* (similar index without the three typically lowest precision elements Mn, P and K). c: HI data that have been corrected using the Student's t distribution based on the number of samples and standards data. The Serocki precision dataset was based on only four analyses (each the mean of five spots), which is why it appears somewhat anomalous in this panel (open diamond).

the latter from the index (termed 'np-HI*') improves the correlation with HI significantly ($R^2 = 0.82$; Fig. 3b). Apparently, the subset of elements in np-HI* preserves aspects of the first-order compositional variability, however, removing incompatible major elements from the index might sacrifice important information. Np-HI and estimated flow volume are not well correlated ($R^2 = 0.25$), although np-HI* and volume are ($R^2 = 0.86$), the scatter in the latter being in the most homogeneous flows. However, precision-normalized HI and estimated flow volumes are even more strongly correlated ($R^2 = 0.964$), which is not a mathematical artifact of the precision-normalization because $\Sigma P_i/n$ of each flow and volume are not correlated ($R^2 = 0.0034$ and 0.069, with and without Mn, P and K, respectively). To summarize, there is a heterogeneity signal in the raw compositional data (uncorrected for analytical precision), but precision-normalization using replicate analyses helps to adjust for variable data quality at the elemental and inter-laboratory scales.

A second issue is how many samples are required to confidently determine the compositional variability within a single lava flow. A sufficient number of sample and standard measurements to encompass the actual data distribution is required to derive a statistically significant measure of the true chemical variation. The appropriate number of samples for S_i is also likely defined in part by flow size and physical morphology, and samples must be spatially well distributed to be representative of the variability length scales within a flow. Many of the existing MOR ($n = 8$–60) and Mauna Loa ($n = 3$–12, except $n = 67$ for the 1984 lava) individual flow datasets are not ideal for this purpose because they are small, as are many of the associated standard replicates ($n = 4$–25 for the MOR unknowns). True variability can theoretically be gleaned from small sample sets using the Student's t distribution, which provides confidence levels from low sample populations by broadening the 2σ width in inverse proportion to the number of samples. Such correction to both S_i and P_i has little effect on most HI values (1–6%); but, HI of the North Cleft Sheet and 1993 Coaxial flows change by $\sim$12%, and Serocki changes by 25%, primarily because P_i is based on only six, seven and four standards, respectively. HI and T-factor-adjusted HI are well correlated ($R^2 = 0.84$, improving to 0.96 without the Serocki datum; Fig. 3c). The basic correlation of estimated flow volume and compositional heterogeneity is unchanged by sample size correction, so small ($n \sim 10$) sample sets may be adequate (although not ideal) to define compositional heterogeneity in typical cases.

A third issue is whether parametric standard deviations [1] are the best mathematical description of compositional (S_i) and analytical (P_i) variability among multiple samples of a single lava flow. This method presumes that chemical variability is normally distributed, which may not be entirely true for variations amongst a group of elements that are at least partially correlated. With extremely small sample datasets displaying limited compositional diversity, it is also possible that some S_i ranges are Poissonian (e.g. dominated by rare 'events'). It is particularly important to test for such behavior because the difficulty with which submarine lava flows are mapped and sampled might lead to accidental inclusion of samples that are actually not from that flow. At the same time, local variations in cooling history may result in real Poissonian distributions if an anomalous sample representing a volumetrically insignificant part of a flow is included in a small dataset.

The importance of 'rare events' in the data was investigated by using ranges (as opposed to standard deviations) for either or both terms in the HI. In each case (HI based on range/range, sdev/range or range/sdev) these heterogeneity indices are only moderately correlated with the normal (sdev/sdev) HI, suggesting that the compositional extremes within the sample and standards data do not dominate the variability signal: range/range slope = 0.90, $R^2 = 0.66$, range/sdev slope = 0.93, $R^2 = 0.76$, sdev/range slope = 0.61, $R^2 = 0.36$. Each of these indices also resulted in a poorer correlation with estimated flow volume. Thus, parametric standard deviations appear to adequately measure S_i and P_i. In undertaking the range analysis we identified and then rejected one spurious lava in the Serocki dataset, changing

HI from 3.53 to 3.27 (sample 1690-5, K/Ti > 200% of the mean of the other 21 samples).

Finally, there is the issue of how many and which elements to include in the HI, which in the present case was limited by the available datasets. More elements can be added but one should consider petrogenetic causes for their variability (see below) because they could weight HI toward measuring a particular cause of heterogeneity. To examine the potential difference between HI based on only major elements (i.e. [26]) versus that including trace elements (i.e. [1]), we have calculated a second HI for the BBQ flow (erupted in 1991 and 1992 near 9°50′N EPR) using six XRF trace elements (Nb, Zr, Sr, V, Y, Rb) as well as the microprobe glass major element data. In this case, the HI values are negligibly different (1.543 and 1.551 with and without trace elements, respectively).

It is extremely difficult to place an error limit on the calculated HI values in Table 1, given the differences in size and quality of the various datasets. Qualitatively, HI values within ~10% or so are probably not distinguishable.

4. Petrological sources of observed compositional heterogeneity

Pre- and post-eruptive low-pressure fractional crystallization during cooling imparts an easily distinguished chemical signature to basaltic lavas (e.g. strong trends on MgO variation diagrams). Data from some flows (e.g. 1993 Coaxial and Cleft Pillow Mounds flows, Fig. 1) display such trends on MgO variation diagrams whereas data from others do not (e.g. 1996 N. Gorda flow, Fig. 1, and Serocki [19]). Compositions of three of the most heterogeneous flows (N. Gorda flow, Cleft Pillow Mounds, and Serocki flows) were modeled to determine the potential effects of low-pressure fractional crystallization, allowing approximation of their relative amounts of crystallization- and non-crystallization-related compositional variability. Early crystallizing assemblages in MORB are typically multi-phase. Simulated constant-pressure liquid evolution paths were generated using the 'Melts' computer program [31] starting with the most undifferentiated (MgO-rich) sample in each flow as parent compositions. Two stage liquid lines of descent (LLDs) best corresponding to observed data trends of each flow were used to 'back-out' crystallization effects on major element compositions of each sample to the parent MgO. The most evolved stage (affecting one or two samples per flow) was a plagioclase–olivine–clinopyroxene fractionation trend; the second portion (affecting most samples) was a plagioclase–olivine fractionation trend.

LLDs were calculated for total pressures ranging from 0.2 to 2.5 kbar, and f_{O2} of 0.1 times the QFM buffer. Slightly different crystallization conditions yielded the 'best' LLD for each flow. Pressures of 0.5, 0.5 and 1.5 kbar best fit the Cleft Pillow Mounds, the 1996 N. Gorda and the Serocki data, respectively. Water content is another important variable, although data exist only for the Cleft Pillow Mounds (0.15 wt% H_2O in the parent; Dixon et al., unpublished data). Higher Al_2O_3 in the N. Gorda and Serocki flows requires slightly higher parent water contents (0.2 wt% and 0.3 wt%, respectively) to prevent plagioclase from being a sole liquidus phase (which would not fit the data trends).

Qualitatively, the Cleft Pillow Mounds samples adhere to the simulated LLD with little scatter, implying that much of the observed heterogeneity may have arisen from low-pressure equilibrium fractional crystallization from a single parent melt. This can be demonstrated quantitatively by a factor of two reduction in the HI of the lava before and after fractionation correction (in both cases HI is calculated without MgO since it is fixed in the fractionation correction, see Table 2).

Both the N. Gorda and Serocki data are more scattered about the constant-pressure LLDs, particularly the Al_2O_3–MgO and CaO–MgO trends, suggesting that they did not crystallize from a single liquid composition. Instead, their arrays may have been formed through mixing of different parental melts and/or more complicated crystallization histories (also noted by [19] for Serocki). This can again be demonstrated quantitatively with the HI of LLD-corrected data, which changed by only 8% (Serocki) and 1% (N. Gorda) in these flows (Table 2).

Thus, although some of the observed intra-flow heterogeneity in some of the highest HI flows can be explained by crystallization, this mechanism cannot be the only control. Instead, other processes (e.g. assimilation, magma recharge, parental magma mixing) likely acted on the pre-erupted magmas.

5. Discussion of global trends

As mentioned previously, within-flow compositional heterogeneity and estimated flow volume are strongly correlated for seven of the 10 MOR lavas in Table 1 ($R^2 = 0.964$). One important question is over what volume range does this correlation hold? No submarine MOR lava flow larger than Serocki has been mapped and sampled to the degree that compositional heterogeneity can be calculated reliably. However, there is indirect evidence that the relationship might flatten out above some critical volume: HI [26] of lavas erupted from 1983 to 1992 in the ongoing Puu Oo eruption of Kilauea ([32] and references therein) is lower than the correlation would predict. Data from the 1783–1784 Laki eruption (Iceland), which produced 14.7 km^3 of lava and 0.4 km^3 (dense rock equivalent) of tephra ([33] and references therein), can also be used to indirectly address this question. We calculated an HI of the basaltic tephra ($n = 51$) using glass compositions analyzed with the University of Hawaii microprobe [33]. No precision data were reported but HI can be estimated from both historical P_i values and using the np-HI* vs. HI correlation (Fig. 3b). This calculation results in tephra HI of 8.1–14.9, using the two estimate methods, respectively (Fig. 2b). The upper HI estimate is close to the value predicted by the HI vs. volume correlation of 14.7 at 0.4 km^3. HI of the lava flow can be likewise estimated to be 7.6–14.7 (very similar to that of the tephra), but there are limited lava data ($n = 13$) and sample coverage of the flow field was very restricted (to primarily near the vent fissures [33]). Although much more data on more geographically dispersed samples are necessary to determine how heterogeneous the entire flow volume is, the well sampled portions of the eruption products have an HI that is 50–100% of that predicted by the HI vs. volume correlation.

Considering the potential sources of error in calculating HI and volumes of MOR flows, it is perhaps remarkable that any global HI–volume correlation exists. The relationship indicates that the pre-solidification history of an erupted batch of lava is generally more complex at larger volume and suggests that many of the same processes affect both the volume and compositional heterogeneity of an MOR eruption. Yet, the three newly analyzed S-EPR lavas do not adhere to this trend within the error limits (Fig. 2). Because HI variations at given volume are most apparent in lavas erupted at ridges with superfast spreading rates, it suggests that volume is not the only scaling parameter for compositional heterogeneity.

HI in the 10 MOR lava flows also varies inversely with spreading rate. Power law regressions to the data yield excellent correlations (Fig. 4).

Table 2
Raw and fractionation-corrected HI data for selected flows

Flow	HI	Number of samples	Highest MgO	HI (no MgO)	HI (LLD-corrected)	HI_{TiFex}
LLD correction						
1996 N. Gorda	2.51	12	8.65	2.01	2.03	1.92
Serocki	3.27	21	8.16	2.97	2.72	2.26
Cleft Pillow Mounds	3.05	12	8.09	2.99	1.48	2.34
LLD correction in £ow subdomains						
Cleft Mound 1	1.37	3		1.38	1.33	
Cleft Mound 5–6	0.23	2		0.24	0.28	
Cleft Mound 8	1.53	6		1.50	0.95	

Fractionation correction along model-estimated LLDs is to highest MgO wt% in each flow (MgO = 'x'). HI 'no MgO' and HI 'LLD-corrected' do not include MgO content as this parameter is fixed in the fractionation correction. Calculations and $TiFe_x$ are explained in the text; HI_{TiFex} is S_i of $TiFe_x$ at x = highest MgO, divided by P_i of TiFe in the precision standards.

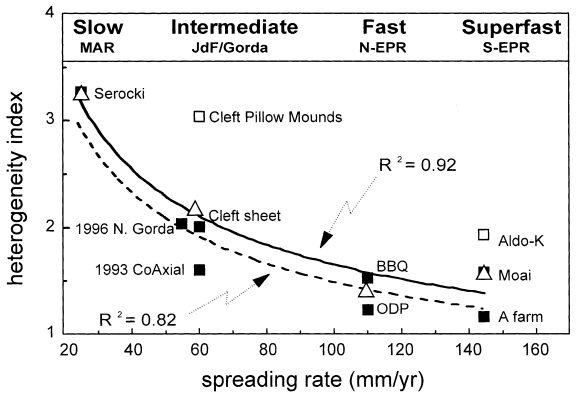

Fig. 4. HI versus spreading rate for 10 individual MOR lava flows (squares). The means for the various spreading rates are also shown (open triangles). Notice the inverse relationship between spreading rate and compositional heterogeneity. Two flows are anomalously heterogeneous for their given spreading rate (open squares) relative to the others (filled squares). The two different power law regressions are described in the text.

Two regressions were calculated in somewhat different manners to help identify outliers: the first (solid line, $R^2 = 0.92$) uses the mean HI at each spreading rate for which we have data and the second (dashed line, $R^2 = 0.82$) uses all the individual flow data except for two anomalously heterogeneous flows (Cleft Pillow Mounds and Aldo-Kihi). Although the dataset is small, both regression curves are functionally very similar, suggesting that the two anomalous flows are true outliers relative to the mean HI at their spreading rate. Both anomalous flows are volumetrically large relative to others at their spreading rate, indicating that very large flows can exceed the typical compositional heterogeneity that is characteristic of a specific spreading rate.

The inter-relationship of HI, volume and spreading rate provides fundamental constraints on MOR magmatic processes. Overall, the development of compositional heterogeneity within an eruptable magma volume and the lava flow it produces reflect variations in how magma accumulates within and is tapped from crustal magma bodies. The volume, shape and compositional range of crustal magma bodies reflect the coupling of magma input and eruption rates, repose period, chamber geometry, crustal strength (thickness, degree of fracturing), and the efficiency of magma cooling/solidification. All depend primarily upon thermal conditions within the upper mantle and MOR crust, the latter of which are controlled by the interplay of the rates of magma supply and loss of heat. To a first approximation, spreading rate can be considered a proxy for magma supply rate (at ridge segments away from the excess melt production of a hot-spot).

Magma enters the crust (continuously or in pulses) with spatial and temporal variations in composition acquired in the source region. In an unevenly cooled magma chamber some or all of this compositional variance can be homogenized and/or overprinted by convection and crystallization. Some subaerial volcanoes approach steady-state wherein erupted volumes are positively correlated with the duration of the preceding repose [34], from which one can generalize that large-volume eruptions will typically require longer melt accumulation periods than small-volume eruptions. In the absence of efficient convective homogenization, longer melt accumulation time should add to the potential for compositional heterogeneity.

In a generic sense, how much magma accumulates at a particular volcano before an eruption takes place reflects a balance of forces driving and preventing eruption, such that eruptions occur when hydrostatic pressure in the reservoir exceeds a critical lithostatic confinement force. Consequently, for magmas of similar volatile content, larger pre-eruptive volumes will accumulate in stronger crust. This probably explains the inverse correlation of MOR lava flow volume and spreading rate [7]. A recent seismic reflection experiment [35] provides additional constraint on maximum volumes of eruptable magma within axial magma chambers along the superfast spreading S-EPR, where magma supply rate is high. Namely, the commonly referred to 'melt lens' contains segregated discontinuous pods of low crystallinity (5–10%) eruptable magma volumes ($\sim 100–200 \times 10^6$ m^3) separated by 15–20 km domains of mostly high crystallinity (40–60%) uneruptable mush [35]. Significantly larger erupted volumes at that spreading rate would likely require recharge during eruption, enhancing compositional heteroge-

neity in the resulting lava flow. Similar constraints have not been established for slower spreading ridges, yet it is likely that the largest-volume eruptions would also require recharge.

Thus the global variations in HI with volume and spreading rate lead to the general conclusion that where the MOR crust is hot and weak, eruptions are likely frequent, smaller and compositionally more homogeneous; where the crust is cold and strong, eruptions are likely to be less frequent and pre-eruptive magma batches should have more opportunities to develop compositional variability. Furthermore, a steady-state eruptable magma lens is more likely to occur beneath a ridge segment as thermal stability, magma supply, and spreading rate increase [36], which should promote compositional homogeneity in erupted lavas. In contrast eruption of more heterogeneous and poorly mixed magma batches should be favored at slower spreading rates.

6. Compositional heterogeneity and flow geography

Local differences in flow morphology can be related to changes in emplacement rate as eruptions progress (e.g. [37,38] and references therein). The geographic distribution of compositional variability within a flow can also be used to help understand emplacement history. Such geographical variability might arise from simultaneous eruption of chemically different lavas from different vents, temporal variability in compositions erupted from a single vent, and/or syn/post-eruptive differentiation. HI in two Mauna Loa flows (1942 and 1950) helps to illustrate the range of conditions that might also apply to MOR eruptions. Both formed in short-duration (2 weeks) eruptions along nearly continuous single eruptive fissures. The compositionally homogeneous (HI = 1.6), moderate-volume 1942 lava formed two sequential flow fields, first erupting from a vent near the summit and then from a $\sim$1 km long fissure some 10 km distant [39]. In contrast, the very compositionally variable (HI = 13.9) high-volume 1950 lava formed in seven major lobes from primitive, intermediate and evolved magmas (11–12, 9–10 and $>$7 wt% MgO) erupted from geographically distinct vents spread over 26 km on the Southeast Rift Zone [40] and required a stratified magma body or multiple, relatively homogeneous magma bodies [1]. Although similar scenarios are difficult to completely resolve for a submarine MOR eruption without fine scale stratigraphic control from direct observation/monitoring or high-resolution age dating, some eruption constraints are provided by geographic distribution of compositional heterogeneity within known lava flows; examples are given below.

6.1. Tubeworm BBQ £ow (EPR)

High-resolution mapping, sampling and ^{210}Po–^{210}Pb dating of this compound lava flow near 9°50′N indicate that lavas were emplaced over $\sim$1 yr between Spring 1991 and January 1992 [9,11] from a nearly continuous 8.5 km long fissure [9], resulting in a relatively homogeneously composed flow [24]. The first eruptive phase was in February–April 1991 [11] (three dated and 15 undated samples were collected by Alvin in April–May 1991). The flow field was reactivated in late December 1991 [11] and produced indistinguishably composed lavas (one dated and two undated samples collected in Spring 1992). HI of lavas from both episodes is 1.55 (see Fig. 5); removing the three 1992-collected samples changes the HI by $<$5%. Two lava pillars from a collapsed part of this flow have a similar HI of 1.57 (based on $\sim$500 elemental analyses at 100 μm spacing on seven transects through glassy pillar crusts [41]).

Lavas were also erupted on the adjacent ridge segment to the north during the second phase of activity: one sample collected from the axis $\sim$5 km north of the main mapped flow (from a feature not present in 1991) erupted in early January 1992 (^{210}Po–^{210}Pb date) and is significantly more compositionally evolved. Adding this sample to the 9°50′N flow field increases the HI by $\sim$20%, indicating that a larger area of the EPR rift was activated during this second phase and multiple magma compositions were erupted, in a geometrically similar fashion to the 1942 and 1950 Mauna Loa eruptions.

6.2. North Cleft Pillow Mounds (JdFR)

This compound lava flow has a strong geographic distribution of compositions along its 17 km length (Fig. 5). All eight mounds (numbered sequentially as M1–M8 from S to N) probably erupted between bathymetric surveys in 1981 and 1987 and although they were not necessarily erupted simultaneously, they are clearly related to a single ≤ 6 yr long volcanic event (possibly ≤ 2 yr [8]). About half of the compositional heterogeneity within this flow is due to low-pressure crystal fractionation (discussed earlier). There is a regular geographical pattern of compositional heterogeneity amongst the mounds, suggesting that each behaved as separate cooling units. MgO content decreases towards the middle (latitudinally) of the flow (Fig. 5). Even with the limited number of samples, it is apparent that the HI values of individual mounds are lower than the HI of the entire flow: HI of M1 and M8 are $\sim 50\%$ of the overall HI (Table 2, Fig. 5). The most compositionally evolved mound (M2) is essentially homogeneous (HI < 1) within the resolution of the limited ($n = 2$) dataset (e.g. analyses are less variable than predicted by the P_i values). After correcting for low-pressure fractionation, the M1 HI changes by only 4%, whereas the M8 HI changes by 63% (to ~ 1, Table 2, Fig. 5). Thus, all of the compositional heterogeneity in the most heterogeneous and volumetrically largest mound (M8) can be ascribed to low-pressure crystal fractionation, but effectively none of the heterogeneity of M1 is related to this process. Instead, M1 appears to be a composite structure with chemical compositions reflecting magma mixing (also inferred independently from trace element data [7,42]).

Overall the geographic distribution of compositional heterogeneity in the mounds is inconsistent with a simple one-time diking and extrusion event. M1 was either built in multiple episodes by lavas of somewhat different composition or erupted from a chemically heterogeneous subridge magma reservoir. The large, LLD-controlled compositional range of M8 is also easiest to rationalize by sequential extrusion of different compositions. Glasses from central mounds M5 and M6 are compositionally more evolved than the other mounds and imply that magmas feeding them either cooled more slowly on the surface (syn/post-emplacement crystallization) or resided longer in crust before eruption (magma chamber crystallization). Because each of the pillow mounds is morphologically similar and thus their extrusion (and cooling) rates should likewise have been similar, we favor a scenario where the M5/M6 lavas acquired their evolved composition prior to eruption. Thus, compositional variations suggest the flow was emplaced from a relatively long fissure by sampling of a horizontally stratified sub-ridge magma lens or lenses, possibly over a few years. Multiple extrusion events can also be inferred from hydrothermal 'mega-plumes' in the water column above the ridge observed in 1986 and 1987 [43].

6.3. North Cleft sheet £ow (JdFR)

This sheet flow was emplaced just to the south of the Cleft Pillow Mounds. It has been mapped as a single contiguous flow with a narrow constriction at 44°58.1′N dividing it into a small northern lobe and broader southern lobe [22,38]. The flow is moderately heterogeneous and lacks a strong geographic variation in composition, although samples have only been recovered from the northern 2/3 of the flow and sample density is lower in the southern portion than in the north (Fig. 5). Magmatic heterogeneities were fairly equally dispersed throughout the flow during eruption, consistent with this being a high emplacement rate sheet flow [22]. Splitting the sample set at 44°58.1′N yields HI values 18% greater (northern domain) and 27% lower (southern domain) than the flow overall. In addition, the most primitive and most evolved compositions occur in the north. Geological mapping suggests the eruptive fissure was confined to the northern half of the sheet flow, that the eruption was longest lived in this area, and that much of the flow south of the constriction was fed from the north [22]. The compositional data also suggest that the northern portion of the flow was active for a longer period of time and the vent(s) sequentially erupted a range of compositions that did not all spread to the south. However, it is also possible that the

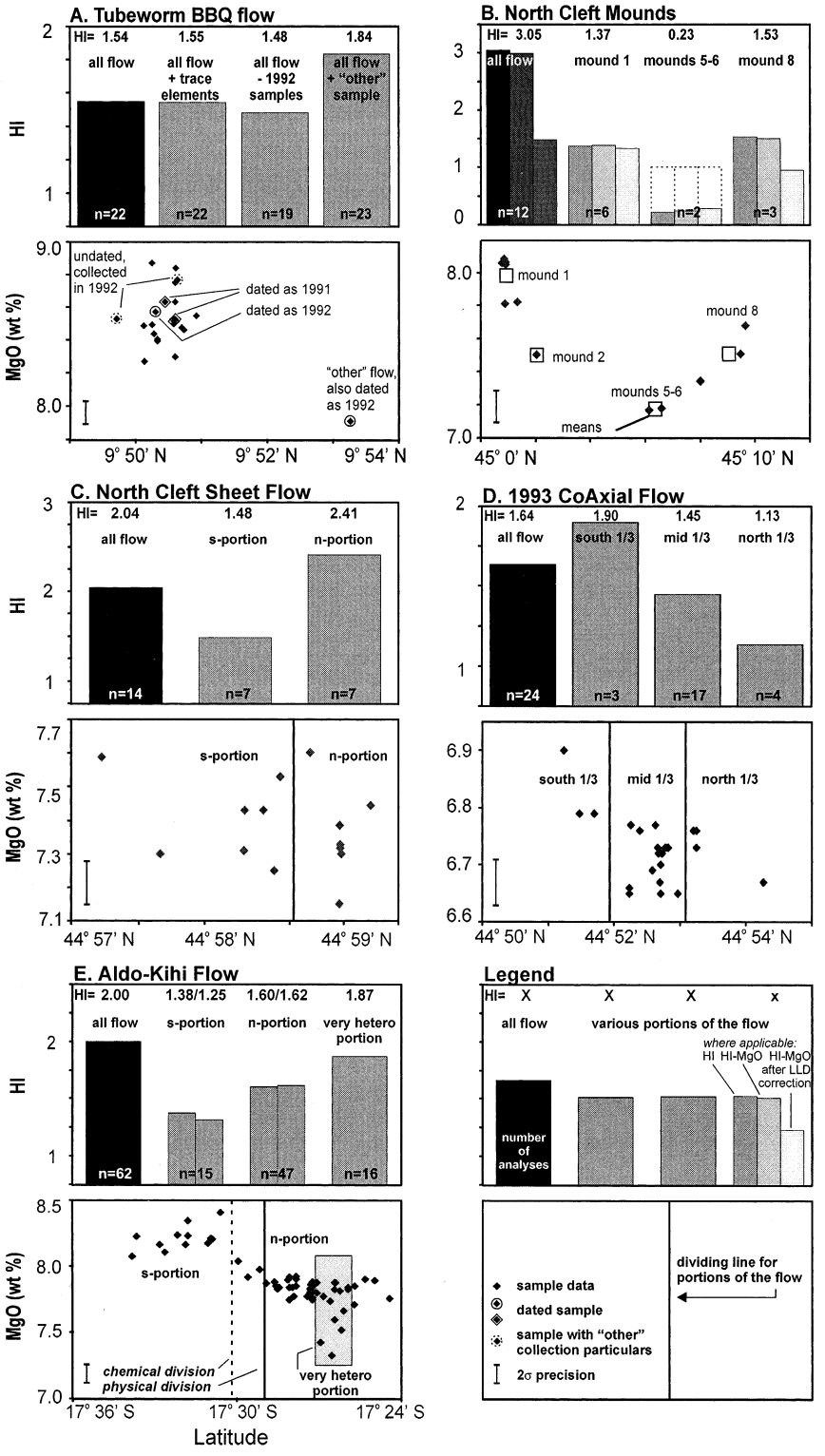
A. Tubeworm BBQ flow
HI= 1.54
1.55
1.48
1.84
all flow
all flow + trace elements
all flow - 1992 samples
all flow + "other" sample
n=22
n=22
n=19
n=23
HI
undated, collected in 1992
dated as 1991
dated as 1992
"other" flow, also dated as 1992
MgO (wt %)
9° 50' N
9° 52' N
9° 54' N
B. North Cleft Mounds
HI= 3.05
1.37
0.23
1.53
all flow
mound 1
mounds 5-6
mound 8
n=12
n=6
n=2
n=3
mound 1
mound 8
mound 2
mounds 5-6
means
45° 0' N
45° 10' N
C. North Cleft Sheet Flow
HI= 2.04
1.48
2.41
all flow
s-portion
n-portion
n=14
n=7
n=7
s-portion
n-portion
44° 57' N
44° 58' N
44° 59' N
D. 1993 CoAxial Flow
HI= 1.64
1.90
1.45
1.13
all flow
south 1/3
mid 1/3
north 1/3
n=24
n=3
n=17
n=4
south 1/3
mid 1/3
north 1/3
44° 50' N
44° 52' N
44° 54' N
E. Aldo-Kihi Flow
HI= 2.00
1.38/1.25
1.60/1.62
1.87
all flow
s-portion
n-portion
very hetero portion
n=62
n=15
n=47
n=16
s-portion
n-portion
chemical division
physical division
very hetero portion
17° 36' S
17° 30' S
17° 24' S
Latitude
Legend
HI= X
X
X
x
all flow
various portions of the flow
where applicable:
HI
HI-MgO
HI-MgO after LLD correction
number of analyses
sample data
dated sample
sample with "other" collection particulars
2σ precision
dividing line for portions of the flow

Fig. 5. HI histograms (HI values given above the columns) and MgO content versus location (filled diamonds) within five MOR lava flows. Geographic variations of compositional heterogeneity in these flows are interpreted in the text. Typical 2σ error is depicted by the vertical bar in each lower panel. A: The Tubeworm BBQ flow data are from samples collected in 1991 and 1992, a subset of which were dated as having erupted in 1991 and 1992. Notice that the lone sample from the next ridge segment to the north (also erupted in 1992) is compositionally distinct. B: The Cleft Pillow Mounds display a regular variation in MgO content on a S–N trajectory through the flow, which consists of eight mounds spread over 17 km of ridge axis. Mean MgO contents for individual mounds are also shown (open squares). Corresponding HI values for the entire flow and for mound 1, mounds 5+6 and mound 8 are shown in the upper panel. This panel includes HI data after fractionation correction to constant MgO, which is why each mound and the overall flow are shown as triplicates of columns. In each case the left-most column represents raw HI, the middle column represents raw HI without MgO, and the right-most column represents LLD-corrected HI values. C: The North Cleft Sheet flow was geographically subdivided based upon flow morphology and there is no obvious geographical variation in composition within it. In contrast, the 1993 Coaxial (D) and Aldo-Kihi (E) flows both show strong geographic variations in composition. The Coaxial flow was subdivided based on chemical groupings. The Aldo-Kihi flow can be geographically subdivided on the basis of flow morphology ('physical division') or flow composition ('chemical division'), with only minor differences in HI (both of which are shown by the doublet columns in the histogram panel for this flow).
←

compositionally heterogeneous magma was supplied all at once to the northern vent(s) and these were mixed during emplacement as the flow spread out from this location.

6.4. 1993 Coaxial £ow (JdFR)

This flow has a strong N–S variation in composition and heterogeneity between flow subdomains (more mafic/more heterogeneous in the south and less mafic/less heterogeneous in the north; Fig. 5) despite its relatively low HI overall. Seismicity propagated northward during this eruption [44], suggesting that the eruption started in the south. It may have first tapped a more mafic and later a more evolved liquid from a compositionally zoned magma body; alternatively, the signature may have arisen during dike propagation, either by fractionation within the dike or by mixing of young mafic and older evolved magma [27]. Similar magma mixing occurred in the early phases of the Puu Oo eruption [32] and accounts for roughly half of the HI value of that flow. The Coaxial flow is a series of coalesced mounds that initially formed from a long eruptive fissure that then localized to a series of vents [23]. The greatest bathymetric anomaly (thickness) is in the south–central portion. Wax modeling of flow morphology suggests that $>50\%$ of the flow volume erupted in 2 h from a 2.5 km long fissure, followed by slower extrusion for 10 days from localized vents [37]. Together, the greater compositional heterogeneity of the southern and middle parts of the flow, slowing effusion rate (inhibiting magma mixing during emplacement) and greater thickness all suggest that vents in the south–central portion of the flow were active for a longer duration.

6.5. Aldo-Kihi £ow (S-EPR)

This flow at 17°30′S has a strong geographic distribution of compositions and lava morphologies along its 8.5 km axial length [13,45,46]. In plan view the flow field is separated into a wide northern portion with en echelon axial collapse troughs and a narrow southern portion lacking a collapse trough. In the north it grades semi-concentrically from high effusion rate jumbled sheets on-axis through lower effusion rate lobate lavas to pillows on the off-axis margins, whereas in the southern portion it is all lobate flows and pillow constructions. Lava compositions are more mafic and less compositionally variable south of 17°30′S (HI is $\sim 35\% <$ HI of the flow overall) and more evolved and more compositionally variable north of 17°30′S (HI is only $\sim 20\% <$ HI of the flow overall; Fig. 5). Splitting the flow morphologically at 17°30′S and splitting the flow on geographic–chemical variations gives only slightly different HI values (Fig. 5). Shibata et al. [46] argued that the compositional pattern formed by northward and southward fractional crystallization at or near the surface from a mafic eruptive center near 17°30′S, noting also that this is not the shallowest or broadest point on the flow. An-

other possibility is that the compositional variations resulted from vertical diking from an along axis compositionally zoned magma body [45]. Neither scenario considers that there is a more chemically heterogeneous subdomain between 17°26′S and 17°27′S characterized by high effusion rate lavas and the most evolved compositions (Fig. 5), the presence of which suggests a third scenario: an initially slow effusion, long fissure eruption expelled mafic lava in the south and unknown composition in the north, followed by vent focusing to a higher effusion rate, primary eruption center between 17°26′S and 17°27′S that expelled a more evolved composition near the end of the eruption. The last phase may have largely covered earlier lavas erupted in the north, making it difficult to distinguish between along axis compositional zonation and a temporal control to the compositional patterns in the flow with existing samples.

7. Implications of within-flow compositional heterogeneity for other MOR petrologic studies

On average, the 10 MOR lava flows in Table 1 are twice as compositionally heterogeneous as the mean precision for major element analysis (mean HI is 2.0). Precision-normalized variability of individual elements can be even greater (up to eight). This range of compositions in individual MOR lava flows indicates that care must be used when interpreting subtle chemical variations between MORB samples with an unknown relationship to individual flow boundaries as being due to spatially, temporally and compositionally distinct eruptions.

Likewise, caution should be used in experiments designed to 'map' magmatic variation through time using MORB compositions from sample grids along and across axis. Two examples of such mapping at 12°N [47] and 9.5–10°N [48] on the EPR used major element oxide compositions (e.g. MgO) and $TiFe_x$. The latter parameter was proposed to sensitively distinguish subtle differences in magma chemistry [47] and is defined as the sum of the differences of $1.5 \times$ Ti and Fe concentrations from their means after Ti and Fe have been low-pressure fractionation-corrected to constant MgO (7.3 wt% [47] and 8.0 wt% [48] in those cases). Variations in Mg, Ti and Fe abundances in both N-MORB datasets are mostly small, but a handful of geochemically distinct transitional or enriched MORBs also occur in both locales. Analytical precision is only given for $TiFe_x$ in those works ($2\sigma = 0.4$), which can be used to show that $TiFe_x$ variability in those entire N-MORB datasets ($2\sigma = 1.1$ and 0.74) is only $\sim$three times [47] and two times [48] the precision. $TiFe_x$ varies over a similar range in the three single flows fractionation-corrected here ($2\sigma = 0.34$, 0.47 and 0.57 in the Cleft Pillow Mounds, 1996 N. Gorda and Serocki flows, respectively). Converting the latter to HI values (S_i/P_i) shows that $TiFe_x$ variability in these three flows is $\sim$two times the analytical precision (see HI_{TiFex} in Table 2). Qualitatively, some of the compositional variability in both EPR sample grids might be due to spatial and temporal variability in magmatic conditions. Yet, because $TiFe_x$ variability is equal to or only slightly greater in the sample grids than in many individual flows, inter-flow and intra-flow compositional variability cannot be confidently resolved, making this form of 'mapping' ambiguous in these cases. $TiFe_x$ and other more subtle chemical variations in these 12°N samples were subsequently used to identify [49] and model [50] a new MORB composition known as 'off-axis' MORB, yet such an exercise seems premature based on the preceding discussion.

8. Summary and future directions

There are many examples of interesting perspectives about magmatic conditions gained by studying individual subaerial lava flows, but logistical difficulties have in the past made this significantly more challenging at submarine volcanoes. Results of this study demonstrate that a great deal can also be learned by studying within-flow compositional heterogeneity in individual MOR lava flows.

1. The strong relationships within the dataset presented here between HI, estimated lava flow

volume and spreading rate suggest that compositional heterogeneity within flows can be used to help decipher global variations in magma supply and thermal conditions at the MOR system. Where the MOR crust is hot and weak, eruptions are likely frequent, smaller and more compositionally homogeneous than where the crust is cold and strong. Addition of more flows to the database and more geochemical tracers would further elucidate the range of MOR magmatic conditions and global crustal accretion variability.

2. Compositional heterogeneity within individual MOR lava flows can be used to study the eruptions that produced them (vent locations, conditions of emplacement). In the optimum, lava sampling and chemical analysis for individual flow studies should be conducted at the highest possible sampling density and spatial coverage. Uncertainty in the results will be minimized with large ($n \geq 30$–50) sample and standard replication datasets. With additional compositional data and detailed physical mapping, it should be possible to further decipher eruptive processes resulting in morphological and compositional domains within a flow. These data, along with hydrothermal vent and faunal distribution maps, should also help to unravel the physiochemical and ecological evolution of newly erupted flows (e.g. cooling history, the development of geothermal circulation, and the colonization of the flow by organisms).
3. Individual flows can be as compositionally variable as regional MOR sample sets. It is therefore important to simultaneously conduct high-resolution geologic mapping and sampling to know the volcanologic context of the samples. With additional compositional data on individual flows from more spreading environments, petrologists will be able to better determine how mantle compositions and melting conditions are mapped into along and across ridge variations in MORB compositions found in samples from geologically un-ma435(int.)-hTJoemondi-var0d

[5] A. Prinzhofer, E. Lewin, C.J. Allègre, Stochastic melting of marble cake mantle: evidence from local study of the East Pacific Rise at 12°50′N, Earth Planet. Sci. Lett. 92 (1989) 189–206.
[6] Y. Niu, D.G. Waggoner, J.M. Sinton, J.J. Mahoney, Mantle source heterogeneity and melting processes beneath seafloor spreading centers: The East Pacific Rise, 18°–19°S, J. Geophys. Res. 101 (1996) 27711–27733.
[7] M.R. Perfit, W.W. Chadwick, Jr., Magmatism at mid-ocean ridges: Constraints from volcanological and geochemical investigations, in: W.R. Buck, P. Delaney, J.A. Karson, Y. Lababrille (Eds.), Faulting and Magmatism at Mid-Ocean Ridges, Geophysical Monograph 106, Am. Geophys. Union, Washington, DC, 1998, pp. 59–115.
[8] W.W. Chadwick Jr., R.W. Embley, C.G. Fox, Evidence for volcanic eruption on the southern Juan de Fuca Ridge between 1981 and 1987, Nature 350 (1991) 416–418.
[9] R.M. Haymon, D.J. Fornari, K.L. Von Damm, M.D. Lilley, M.R. Perfit, J.M. Edmond, W.C.I. Shanks, R.A. Lutz, J.M. Grebmeier, S. Carbotte, D. Wright, E. McLaughlin, M. Smith, N. Beedle, E. Olson, Volcanic eruption of the mid-ocean ridge along the East Pacific Rise crest at 9 degrees 45–52′N; direct submersible observations of seafloor phenomena associated with an eruption event in April, 1991, Earth Planet. Sci. Lett. 119 (1993) 85–101.
[10] W.W. Chadwick Jr., R.W. Embley, Lava flows from a mid-1980s submarine eruption on the Cleft Segment, Juan de Fuca Ridge, J. Geophys. Res. 99 (1994) 4761–4776.
[11] K.H. Rubin, J.D. Macdougall, M.R. Perfit, ^{210}Po–^{210}Pb dating of recent volcanic eruptions on the sea floor, Nature 368 (1994) 841–844.
[12] C.G. Fox, W.E. Radford, R.P. Dziak, T.K. Lau, H. Matsumoto, A.E. Schreiner, Acoustic detection of a seafloor spreading episode on the Juan de Fuca Ridge using military hydrophone arrays, Geophys. Res. Lett. 22 (1995) 131–134.
[13] J. Sinton, E. Bergmanis, K.H. Rubin, R. Batiza, T.K.P. Gregg, K. Grönvold, S. White, K. Macdonald, Volcanic eruptions at superfast spreading: the East Pacific Rise, 17°–19°S, J. Geophys. Res. (2001), submitted.
[14] G.P.L. Walker, Compound and simple lava flows and flood basalts, Bull. Volcanol. 35 (1971) 579–590.
[15] S. Self, T. Thordarson, L. Keszthelyi, Emplacement of continental flood basalt lava flows, in: J.J. Mahoney, M.F. Coffin (Eds.), Large Igneous Provinces: Continental, Oceanic and Planetary Flood Volcanism, Geophysical Monograph 100, Am. Geophys. Union, Washington, DC, 1997, pp. 381–410.
[16] J.R. Carden, A.W. Laughlin, Petrochemical variations within the McCartys basalt flow, Valencia County, New Mexico, GSA Bull. 85 (1974) 1479–1484.
[17] M.M. Lindstrom, L.A. Haskin, Causes of compositional variations within mare basalt suites, Proc. 9th Lunar Planet. Sci Conf., 1978, pp. 466–486.
[18] M.M. Lindstrom, L.A. Haskin, Compositional inhomogeneities in a single Icelandic tholeiite flow, Geochim. Cosmochim. Acta 45 (1981) 15–31.
[19] S.E. Humphris, W.B. Bryan, G. Thompson, L.K. Autio, Morphology, geochemistry, and evolution of Serocki volcano, Ocean Drilling Program, 106/109, College Station, TX, 1990, pp. 67–84.
[20] R.W. Embley, W.W. Chadwick Jr., M.R. Perfit, E.T. Baker, Geology of the northern Cleft segment, Juan de Fuca Ridge: Recent lava flows, sea-floor spreading, and the formation of megaplumes, Geology 19 (1991) 771–775.
[21] W.B. Bryan, S.E. Humphris, G. Thompson, J.F. Casey, Comparative volcanology of small axial eruptive centers in the MARK area, J. Geophys. Res. 99 (1994) 2973–2984.
[22] R.W. Embley, W.W. Chadwick Jr., Volcanic and hydrothermal processes associated with a recent phase of seafloor spreading at the northern Cleft segment: Juan de Fuca Ridge, J. Geophys. Res. 99 (1994) 4741–4760.
[23] W.W. Chadwick Jr., R.W. Embley, C.G. Fox, SeaBeam depth changes associated with recent lava flows, CoAxial segment, Juan de Fuca Ridge: Evidence for multiple eruptions between 1981–1993, Geophys. Res. Lett. 22 (1995) 167–170.
[24] T.K.P. Gregg, D.J. Fornari, M.R. Perfit, R.M. Haymon, J.H. Fink, Rapid emplacement of a mid-ocean ridge lava flow on the East Pacific Rise at 9° 46′–51′N, Earth Planet. Sci. Lett. 144 (1996) E1–E7.
[25] W.W. Chadwick Jr., R.W. Embley, T.M. Shank, The 1996 Gorda Ridge eruption: Geologic mapping, sidescan sonar, and SeaBeam comparison results, Deep-Sea Res. II 45 (1998) 2547–2569.
[26] K.H. Rubin, M.C. Smith, M.R. Perfit, D.M. Christie, L.F. Sacks, Geochronology and petrology of lavas from the 1996 North Gorda Ridge eruption, Deep-Sea Res. II 45 (1998) 2571–2597.
[27] M.C. Smith, Geochemistry of Eastern Pacific MORB: Implications for MORB Petrogenesis and the Nature of Crustal Accretion Within the Neovolcanic Zones of Two Recently Active Ridge Segments, Ph.D. thesis, University of Florida, FL, 1999.
[28] J.M. Sinton, Eruptive history of the Hengill volcanic system: mid-atlantic ridge in the Western Rift Zone of Iceland, EOS Trans. Am. Geophys. Union 78 (1997) F645.
[29] J.P. Lockwood, P.W. Lipman, Holocene eruptive history of Mauna Loa volcano, US Geol. Surv. Prof. Pap. 1350 (1987) 509–536.
[30] J.M. Rhodes, Geochemistry of the 1984 Mauna Loa eruption: Implications for magma storage and supply, J. Geophys. Res. 93 (1988) 4453–4466.
[31] M.S. Ghiorso, R.O. Sack, Chemical mass transfer in magmatic systems IV. A revised and internally consistent thermodynamic model for the interpolation and extrapolation of liquid–solid equilibria in magmatic systems at elevated temperatures and pressures, Contrib. Mineral. Petrol. 119 (1995) 197–212.
[32] M. Garcia, J.M. Rhodes, F.A. Trusdell, A. Pietruszka,

Petrology of lavas from the Puu Oo eruption of Kilauea Volcano: III. The Pond stage (1986–1992), Bull. Volcanol. 58 (1996) 359–379.
[33] Th. Thordarsson, S. Self, N. Óskarsson, T. Hulsebosch, Sulfur, chlorine, and fluorine degassing and atmospheric loading by the 1783–1884 AD Laki Skaftár Fires eruption in Iceland, Bull. Volcanol. 58 (1996) 205–225.
[34] G. Wadge, Steady state volcanism: evidence from eruption histories of polygenetic volcanoes, J. Geophys. Res. 87 (1982) 4035–4049.
[35] S.C. Singh, G.M. Kent, J.S. Collier, A.J. Harding, J.A. Orcutt, Melt to mush variations in crustal magma properties along the ridge crest at the southern East Pacific Rise, Nature 394 (1998) 874–878.
[36] J.M. Sinton, R.S. Detrick, Mid-ocean ridge magma chambers, J. Geophys. Res. 97 (1992) 197–216.
[37] T.K.P. Gregg, J.H. Fink, Quantification of submarine lava-flow morphology through analog experiments, Geology 23 (1995) 73–76.
[38] W.W. Chadwick Jr., T.K.P. Gregg, R.W. Embley, Submarine lineated sheet flows: a unique lava morphology formed on subsiding lava ponds, Bull. Volcanol. 61 (1999) 194–206.
[39] G.A. Macdonald, The 1942 eruption of Mauna Loa, Hawaii, Am. J. Sci. 241 (1943) 241–256.
[40] G.A. Macdonald, Activity of Hawaiian volcanoes during the years 1940–50, Bull. Volcanol. 15 (1954) 119–179.
[41] T.K.P. Gregg, D.J. Fornari, M.R. Perfit, W.I. Ridley, M.D. Kurz, Using submarine lava pillars to record mid-ocean ridge eruption dynamics, Earth Planet. Sci. Lett. 178 (2000) 195–214.
[42] M.C. Smith, M.R. Perfit, I.R. Jonasson, Petrology and geochemistry of basalts from the southern Juan de Fuca Ridge: Controls on the spatial and temporal evolution of mid-ocean ridge basalt, J. Geophys. Res. 99 (1994) 4787–4812.
[43] E.T. Baker, J.W. Lavelle, R.A. Feely, G.J. Massoth, S.L. Walker, J.E. Lupton, Episodic venting of hydrothermal fluids from the Juan de Fuca Ridge, J. Geophys. Res. 94 (1989) 9237–9250.
[44] R.P. Dziak, C.G. Fox, A.E. Schreiner, The June–July 1993 seismo-acoustic event at CoAxial segment, Juan de Fuca Ridge: Evidence for a lateral dike injection, Geophys. Res. Lett. 22 (1995) 135–138.
[45] E.C. Bergmanis, J.M. Sinton, S. White, K.C. Macdonald, R. Batiza, K. Rubin, T. Gregg, C. Van Dover, K. Grönvold, Anatomy of a mid-ocean ridge volcanic eruption: the Aldo-Kihi flow between 17°24′ and 17°34′S, East Pacific Rise, Trans. Am. Geophys. Union 80 (1999) F1075.
[46] T. Shibata, O. Okano, R.W. Embley, K. Nogami, K. Fujioka, K. Sayanagi, M. Kinoshita, Along-axis fractionation of basalts: samples from recent lava flows at 17°24–35′S, East Pacific Rise, Trans. Am. Geophys. Union 80 (1999) F1075.
[47] J.R. Reynolds, C.H. Langmuir, J.F. Bender, K.A. Kastens, W.B.F. Ryan, Spatial and temporal variability in the geochemistry of basalts from the East Pacific Rise, Nature 359 (1992) 493–499.
[48] M.R. Perfit, D.J. Fornari, M.C. Smith, J.F. Bender, C.H. Langmuir, R.M. Haymon, Small-scale spatial and temporal variations in mid-ocean ridge crest magmatic processes, Geology 22 (1994) 375–379.
[49] J.R. Reynolds, C.H. Langmuir, Identification and implications of off-axis lava flows around the East Pacific Rise, Geochem. Geophys. Geosyst. G^3 1 (2000).
[50] M. Spiegelman, J.R. Reynolds, Combined dynamic and geochemical evidence for convergent melt flow beneath the East Pacific Rise, Nature 402 (1999) 282–285.

Analytical and Geological Metadata for some MOR lava flows:

A brief account of each lava flow discussed in Rubin et al., 2001 and additional details about compositional analyses are presented here. Further details of lava volume estimates in Table 1 can be found in [24] (BBQ Flow), [23] (Cleft Pillow Mounds, 1993 Coaxial Flow, 1996 Gorda Flow), [7] (Serocki, ODP, and Cleft Sheet Flow), and [13] (Moai, Animal Farm and Aldo-Kihi flows). Reference numbers refer to those in the manuscript, plus numbers A1 to A10 below.

Flow Name	Axial Length (km)	Area (km^2)	Chemical Analysis details:	Other Flow details:
1993 CoAxial	~3.8	~0.7	Geochemical analyses of 24 samples of this flow are in [27]. Analytical precisions (P_i) are based on 7 in-run replicate analyses of the JdF-D2 MORB standard.	Pillow to lobate flow aligned with the ridge-axis [25]. Time of emplacement is constrained by seismic, geologic and bathymetric evidence as June-July of 1993 [12, 25]. This flow is believed to be the erupted manifestation of the dike that propagated up to 60 km along axis from south to north [44]. Besides the main flow, at least 3 small isolated occurrences of the 1993 lava occur <1 km north of the main flow within a syneruptive graben. Samples (collected in situ by submersible and ROV) are geographically well-distributed
Cleft Pillow Mounds	17	2.8	Analytical data (Smith and Perfit, unpublished) are available from the authors. P_i data are taken as the average precision of 3 different in-run MORB standard glasses (Jdf-D2, USNM, 2392-9: 11, 5, 9 analyses respectively [27]).	This flow is an array of 8 discontinuous pillow lava mounds arranged parallel to ridge-strike [8, 25]. Emplacement time is constrained by repeat bathymetric surveys to be between 1981 and 1991, most likely after 1983 [8]. Geographic distribution of the samples is representative of the entire length of the flow. Data from 12 samples were used (11 collected in situ by submersible and 1 by dredge).
Cleft Sheet	~7.5	~4.2	Geochemical analyses are described in [42]. Analytical precision was based on 6 in-run replicate analyses of the VG2 MORB standard.	Lineated to jumbled sheet flow with minor lobate domains erupted from a fissure in the northern 1 km of the flow (minor eruptive vents may also extend 4 km to the south), with lava flowing southward [7, 20, 22]. Flow morphology details in [A1]. Eruption timing is poorly constrained: circumstantial evidence suggests the flow is very young, but sidescan sonar data indicate that it erupted prior to 1982 [22]. Samples were collected in situ by submersible in 1988 ([42] and unpublished). No samples have been collected from the southern ~3 km of this flow and existing data is biased towards its northern half. Seven samples collected in 1990 from a limited geographical area fall within the range of the other data, but lack P_i data, so are not included here.
N. Gorda	2.6	~0.76	Geochemical analyses from [26]. Precision data are based on 20 replicates of VG2 analyzed during the approximate time frame of the "unknown" analyses (R. Nielson, pers. comm).	Eruption timing of this long pillow mound flow [25] is constrained seismically and radiometrically to be in early 1996 [26, A2]. Data from 12 samples were analyzed (collected in situ from the northern portion of the flow by ROV or deep-tow camera) [26]. Sample distribution is geographically limited and may not be representative of the entire flow. Ridge segment fields in Fig. 1 from [A3, A4]
Tube-worm BBQ	~8	~0.72	Analytical data are based on the same 21 samples as in [24]; minor differences between compositional averages and standard deviations here and in [24] are due to subsequent reanalysis of some samples (Perfit et al., unpub. data). Precision data are based on 24 in-run replicate analyses of JdF-D2. HI of 1.57 from the lava pillar study [41] does not include spot analysis data from 1 mm thick anomalous-composition bands near the tops of 2 pillars	This flow exhibits a variety of sheet and lobate morphologies extending from ~9°46' to 9°51' N. The flow is interpreted to have erupted from a nearly continuous eruptive fissure [24] in early 1991 based on submersible observations [9] and radiometric dating [11]. It has been suggested that the BBQ flow was largely contained within a preexisting axial summit collapse trough [24]. High resolution radiometric dating confirms that at least one sample included in the database was erupted during a second phase of eruptive activity in late 1991 or early 1992 [11]. Note that the geographical distribution of samples in [24] and here is from ~9°49.7' to 9°50.9' N, and thus is not necessarily representative of the entire flow [24].

Flow Name	Axial Length (km)	Area (km^2)	Chemical Analysis details:	Other Flow details:
ODP	0.26	0.005 to 0.021	Analytical data are based on 2 sets of 4 analyses conducted at different institutions [A7, A8]. Minor corrections were made to the [A8] data to normalize for a slight data offset (in FeO, MgO, CaO, Na_2O and P_2O_5 concentrations) between the data sets Average HI for each set of four analyses differs from the HI index calculated from the combined set by <15%. In-run standards analyses were unavailable so historical VG2 data from the Univ. of Hawaii microprobe were used.	Ponded sheet flow drilled on ODP leg 142, site 864. It is the uppermost of at least two different units identified at this drill site. Mapping constraints for this flow are not as strong as some of the other flows discussed here, but the flow is thought to be ~260 m long and 20-80 meters wide [A5, A6]. It appears to have been restricted to within the axial summit collapse trough, the best thickness estimate is 3.5 m, but may be as great as 12 m [A7]. Taking this into account, estimated flow volumes used in Table 1 are likely minimum estimates (by up to factor of 4). Both the small volume of this flow (even considering the maximum probable volume) and the manner of emplacement (as a small area, relatively featureless ponded flow) make this flow the morphological end member of the flows considered here (Serocki is the other end member). Samples are limited to one geographic location (but a range of depths within the flow), and might underestimate the true heterogeneity in this flow.
Moai	~7.5	~3.3	Analysis of 11 samples and 10 in-run replicate analyses of VG2 for P_i values from (Bergmanis et al. unpub. data).	Largely composed of jumbled sheet flows confined to within a structural graben [13]. The timing of the eruption is poorly constrained, but it is considered to postdate tectonic features identified within the graben. Samples were collected in situ by submersible throughout the flow [13].
Animal Farm	~15	~17	Analysis of 59 samples and 17 in-run replicate analyses of VG2 for P_i values from (Bergmanis et al., unpub. data).	This flow is comprised of a range of lava morphologies, dominated by sheet flows in its center and lobate to pillowed forms at its edges [13]. Timing of the eruption is suggested to be within the last century based on observational data, and possibly within the past few decades [13]. Samples were collected in situ by submersible throughout the flow [13].
Aldo-Kihi	~18.5	~14	Analysis of 60 samples and 18 in-run replicate analyses of VG2 for P_i values from (Bergmanis et al., unpub. data).	This flow has been studied by two different research groups [13, 45, 46, A9]. Lava morphologies range from jumbled sheets to pillows and show some correlation to geography [13]. Observational data suggest that this flow may have been emplaced within the past 2 decades [13] and compositions of buoyant hydrothermal plumes in the water column above the ridge suggest the eruption may have occurred "several years" prior to 1993 [A9]. Samples were collected in situ by submersible throughout the flow [13].
Serocki Volcano	0.8	0.5	Analysis of 21 [19] samples and 4 in-run replicate analyses of VG2 for P_i values (T. O'hearn, unpublished data). Note that one sample recovered by submersible was excluded from the Serocki database for reasons discussed in the text.	A small roughly circular volcanic construct rising 60m above surrounding terrain and a ~800m diameter at its summit plateau [19, 21]. Timing of eruption is poorly constrained, although it has been suggested that Serocki volcanism may be several tens of thousands of years old [A10]. Geologic and geochemical data suggest that this is a composite "flow", having formed during at least two separate phases of volcanic activity, and it includes a variety of lava forms [19]. It is one of the best examples of detailed fine-scale sampling of a probable single eruptive unit on the MAR. Samples are well-distributed in the flow and were recovered in situ by submersible [19].

Additional References

A1. W. W. Chadwick, Jr., R. W. Embley, D. S. Scheirer, H. P. Johnson. High-resolution bathymetric surveys using scanning sonars: relationships between hydrothermal vents and geologic structure at recent eruption sites on the Juan de Fuca Ridge, J. Geophys. Res., in review.

A2. C. G. Fox and R. P. Dziak, Hydroacoustic detection of volcanic activity on the Gorda Ridge, February-March 1996, Deep-Sea Res. II 45 (1998) 2513-2530.

A3. A. S. Davis, D. A. Clague (1987) Geochemistry, mineralogy, and petrogenesis of basalt from the Gorda Ridge, J. Geophys. Res., 92, 10467-10483.

A4. A. S. Davis, D. A. Clague (1990) Gabbroic xenoliths from the northern Gorda Ridge: Implications for magma chamber processes, J. Geophys. Res., 95, 10885-10906.

A5. Shipboard Engineering and Scientific Parties, 2. Introduction, Background, and Scientific Objectives: Engineering Leg 142 at the East Pacific Rise In: Proceedings of the Ocean Drilling Program V. 142, Initial Reports (Eds: R. Batiza, M. A. Storms, and J. F. Allen) Ocean Drilling Program, College Station, Tx (1993) 31-40.

A6. D. J. Fornari, R. M. Haymon, M. R. Perfit, T. K. P. Gregg, and M. H. Edwards, Axial summit trough of the East Pacific Rise 9°N to 10°N: Geological characteristics and evolution of the axial zone on fast-spreading mid-ocean ridges, J. Geophys. Res. 103 (1998) 9827-9855.

A7. R. Batiza, J. F. Allan, W. Bach, K. Boström, J. G. Brophy, G. J. Fryer, S. J. Goldstein, K. Harpp, R. M. Haymon, R. Hekinian, J. E. Johnston, Y. Niu, and B. G. Poylak, Petrology, chemistry and petrogenesis of Leg 142 basalts - synthesis of results. In: Proceedings of the Ocean Drilling Program V. 142, Scientific Results (Eds: R. Batiza, M. A. Storms, and J. F. Allen) Ocean Drilling Program, College Station, Tx (1995) 3-8.

A8. A. Artamonov, N. Suschevskaya, B. Zolotarev, G. Kashinev, and V. Kurnosov, Geochemistry of basalts from the East Pacific Rise axis zone at 9°30.45'N, Leg 142. In: Proceedings of the Ocean Drilling Program V. 142, Scientific Results (Eds: R. Batiza, M. A. Storms, and J. F. Allen) Ocean Drilling Program, College Station, Tx (1995) 75-81.

A9. R.W. Embley, J.E. Lupton, G.Massoth, T.Urabe, V. Tunnicliffe, D.A. Butterfield, T. Shibata, O. Okano, M. Kinoshita, K. Fujioka, Geological, chemical, and biological evidence for recent volcanism at 17.5°S: East Pacific Rise. Earth Planet. Sci. Lett. 163 (1998) 131-147.

A10 J. A. Karson, G. Thompson, S. E. Humphris, J. M. Edmond, W. B. Bryan, J. R. Brown, A. T. Winters, R. A. Pockalny, J. R. Casey, A. C. Campbell, G. Klinkhammer, M. R. Palmer, R. J. Kinzler, and M. M. Sulanowska, Along-axis variations in seafloor spreading in the MARK area, Nature 328 (1987) 681-685.